Earth and Space Science

RESEARCH ARTICLE
10.1029/2019EA000799

# Role of Ammonia on the Feedback Between AWC and Inorganic Aerosol Formation During Heavy Pollution in the North China Plain

**Baozhu Ge[1], Xiaobin Xu[2], Zhiqiang Ma[3], Xiaole Pan[1], Zhe Wang[1,4], Weili Lin[5], Bin Ouyang[6], Danhui Xu[1,9], James Lee[7], Mei Zheng[8], Dongsheng Ji[1], Yele Sun[1], Huabin Dong[8], Freya Anne Squires[7], Pingqing Fu[1], and Zifa Wang[1,9,10]**

[1]State Key Laboratory of Atmospheric Boundary Layer Physics and Atmospheric Chemistry, Institute of Atmospheric Physics, Chinese Academy of Sciences, Beijing, China, [2]State Key Laboratory of Severe Weather and Key Laboratory for Atmospheric Chemistry of China Meteorological Administration, Chinese Academy of Meteorological Sciences, Beijing, China, [3]Institute of Urban Meteorology, China Meteorological Administration, Beijing, China, [4]Research Institute for Applied Mechanics, Kyushu University, Fukuoka, Japan, [5]College of Life and Environmental Sciences, Minzu University of China, Beijing, China, [6]Lancaster Environment Centre, Lancaster University, Lancaster, UK, [7]National Centre for Atmospheric Science Department of Chemistry, University of York, York, UK, [8]State Key Joint Laboratory of Environmental Simulation and Pollution Control, College of Environmental Sciences and Engineering, Peking University, Beijing, China, [9]University of Chinese Academy of Sciences, Beijing, China, [10]Center for Excellence in Regional Atmospheric Environment, Institute of Urban Environment, Chinese Academy of Sciences, Xiamen, China

**Key Points:**
- Ambient $NH_3$ and related species were measured and simulated at high resolutions during the wintertime APHH-Beijing campaign in 2016
- Total $NH_x$ was mostly in excess of the $SO_4^{2-}$-$NO_3^-$-$NH_4^+$-water equilibrium system in NCP
- $NH_4NO_3$ is the most important factor driving the formation of AWC and promotes the positive feedback of AWC and SIA reactions

**Supporting Information:**
- Supporting Information S1

**Correspondence to:**
B. Ge, X. Xu and Z. Wang,
gebz@mail.iap.ac.cn;
xiaobin_xu@189.cn;
zifawang@mail.iap.ac.cn

**Citation:**
Ge, B., Xu, X., Ma, Z., Pan, X., Wang, Z., Lin, W., et al. (2019). Role of ammonia on the feedback between AWC and inorganic aerosol formation during heavy pollution in NCP. *Earth and Space Science*, *6*, 1675–1693. https://doi.org/10.1029/2019EA000799

Received 26 JUL 2019
Accepted 24 AUG 2019
Accepted article online 29 AUG 2019
Published online 12 SEP 2019



**Abstract** Atmospheric $NH_3$ plays a vital role not only in the environmental ecosystem but also in atmosphere chemistry. To further understand the effects of $NH_3$ on the formation of haze pollution in Beijing, ambient $NH_3$ and related species were measured and simulated at high resolutions during the wintertime Air Pollution and Human Health-Beijing (APHH-Beijing) campaign in 2016. We found that the total $NH_x$ (gaseous $NH_3$+particle $NH_4^+$) was mostly in excess of the $SO_4^{2-}$-$NO_3^-$-$NH_4^+$-water equilibrium system during our campaign. This $NH_x$ excess made medium aerosol acidity, with the median pH value being 3.6 and 4.5 for polluted and nonpolluted conditions, respectively, and enhanced the formation of particle phase nitrate. Our analysis suggests that $NH_4NO_3$ is the most important factor driving the increasing of aerosol water content with $NO_3^-$ controlling the prior pollution stage and $NH_4^+$ the most polluted stage. Increased formation of $NH_4NO_3$ under excess $NH_x$, especially during the nighttime, may trigger the decreasing of aerosol deliquescence relative humidity even down to less than 50% and hence lead to hygroscopic growth even under RH conditions lower than 50% and the wet aerosol particles become better medium for rapid heterogeneous reactions. A further increase of RH promotes the positive feedback "aerosol water content-heterogeneous reactions" and ultimately leads to the formation of severe haze. Modeling results by Nested Air Quality Prediction Monitor System (NAQPMS) show the control of 20% $NH_3$ emission may affect 5–11% of particulate matter $PM_{2.5}$ formation under current emissions conditions in the North China Plain.

## 1. Introduction

Ammonia ($NH_3$) is an alkaline gas that plays a very important role in the atmosphere. It may react with acidic species such as sulfuric and nitric acids to form ammonium salts (Walker et al., 2004), which are the major inorganic components of fine particles and contribute to regional haze (Cao et al., 2009; Fu et al., 2017; Meng et al., 2018). In addition, $NH_3$ is one of the major constitutes of reduced nitrogen and can cause significant acidification of the ecosystems (Hernandez et al., 2016; Liu et al., 2013; Pan et al., 2012; Sheppard et al., 2011).

Although the China government has made tremendous efforts on the control of the $SO_2$ and $NO_x$ emissions since 2005 (Wang & Hao, 2012; Xia et al., 2016), little attention has been paid to $NH_3$ control. As a result, atmospheric $NH_3$ experienced a significant increasing trend. For example, Warner et al. (2017) reported an increased trend of $NH_3$ vertical column density over agricultural regions across China (2.3%/year) based on satellite observation between 2002 and 2013. Fu et al. (2017) also found an obvious increase of $NH_3$ vertical column density in recent years (from 2011 to 2014) over magecity clusters of the North China Plain

(NCP), the Yangtze River Delta, and the Pearl River Delta. The increase in atmospheric $NH_3$ is believed to the benefits of the reduction in $SO_2$ and $NO_x$ emissions (Lachatre et al., 2019; Liu et al., 2018), especially in East China (Fu et al., 2017). Several studies revealed the importance of $NH_3$ to the formation of secondary inorganic aerosols (SIAs; Cao et al., 2009; Meng et al., 2018) and organic aerosols as well (Bin Babar et al., 2017; Na et al., 2007). However, the mechanisms that $NH_3$ promotes the formation of secondary aerosols are still controversial. Cheng et al. (2016) indicate that the fast transform of gaseous $SO_2$ to particle $SO_4^{2-}$ under the polluted conditions is due to the neutralization of $NH_3$, which raises particle pH and thereby facilitated the aqueous oxidation of $HSO_3^-/SO_3^{2-}$ by $NO_2$. Using the reverse mode of ISORROPIA II model, Wang et al. (2016) estimated the aerosol acidity and found that the neutralization of $NH_3$ could result in a neutral aerosol with pH≈7. On the contrary, Song et al. (2018) stated the forward mode calculations would be superior to the reverse one and obtained a moderate acidity (pH≈4–5) for fine particles under the winter haze conditions in the NCP, which is consistent with that reported by Liu et al. (2017). The forward mode can solve the total (gas + aerosol) concentration of each species, while the reverse mode only use the concentration of each species in the aerosol phase as input.

One of the factors limiting our ability to quantify the effects of $NH_3$ on aerosols formation in China is the lack of well-designed observations, focusing on gas-particle conversions involving $NH_3$, $SO_2$, $NO_x$, etc. Although some networked observations of ambient $NH_3$ have been conducted (Meng et al., 2010; Pan et al., 2018) using passive $NH_3$ sampling techniques, the time resolutions were too low to study aerosol formation. Recently, some high temporal resolution measurements of $NH_3$ and other species related to aerosol formation became available and allowed for studying the aerosol acidity (Liu et al., 2017), the formations of SIA (Cao et al., 2009; Meng et al., 2018), and secondary organic aerosol (Bin Babar et al., 2017; Na et al., 2007). Excess $NH_x$ ($NH_3$+$NH_4^+$) in the aerosol equivalent system is often used to distinguish the pathway of ammonium sulfate as well as the ammonium nitrate in $PM_{2.5}$ (He et al., 2012; Liu et al., 2017; Pathak et al., 2009). In this study, high-resolution measurements of $NH_3$ as well as other related species during the APHH-Beijing campaign are analyzed. The impacts of excess $NH_x$ on the gas-particle partition and inorganic aerosol formation during heavy pollution and clean episodes are investigated. The results will improve our understanding of the role of $NH_3$ in aerosol formation in China and thus provide some scientific basis for government regulations aiming to reduce regional haze, acid deposition, and ultimately improve the ecosystem and environment.

## 2. Method

### 2.1. Field Measurement Site

The APHH-Beijing winter campaign was performed from 10 November to 10 December 2016 at the Institute of Atmospheric Physics (IAP), Chinese Academy of Sciences (39°58′28″N, 116°22′16″E), which is located between the north 3rd and 4th Ring Road in Beijing. The IAP site is a typical urban site with influences from local traffic and cooking sources (Sun et al., 2012). The prevailing winds during the observation period were south-westerly and northerly. A study by Ge et al. (2018) shows that the southerly wind transports the polluted air masses into Beijing with a regional transport contribution of almost 40% to fine particles pollution on yearly average.

### 2.2. Continuous Hourly Measurement of Composition of $PM_{2.5}$ and Its Related Species

In this study, continuous dichotomous aerosol chemical speciation analyzer (Model ACSA-14; Kimoto Electric, Ltd., Japan) was deployed to measure the two main water-soluble inorganic ions ($NO_3^-$ and $SO_4^{2-}$), optical black carbon, water soluble organic carbon, aerosol acidity and aerosol water content (AWC). Briefly, the $NO_3^-$ and $SO_4^{2-}$ are measured on the basis of ultraviolet/visible absorption spectrometry at around 200 nm and turbidimetry with 20 ml of 0.5-M barium chloride ($BaCl_2$) solution added to the sample, respectively. Duan et al. (2016) reported a good consistency with high value of $R^2$ (0.99) and a slope of 0.97 between ACSA and the offline samples method in winter of Beijing. The aerosol acidity was measured based on change of the bromophenol blue visible absorption spectrum by adding 8 ml of 1.5-mM bromophenol blue solution to the sample. A strong consistency between the measured and calculated $H^+$ were reported by Duan et al. (2016). More details of the procedure for measuring aerosol acidity were discussed in a previous study by King and Kester (1989). Dry and wet $PM_{2.5}$ were also measured by ACSA; AWC

can be calculated by subtracting the masses of dried aerosols from those of wet aerosols (i.e., not dried). The detection limits for $NO_3^-$, $SO_4^{2-}$, $H^+$, and AWC are 3 nmol/m$^3$, 15 nmol/m$^3$, 10 nmol/m$^3$, and 2 μg/m$^3$, respectively.

The other water-soluble inorganic components (i.e., $NH_4^+$, $Cl^-$, $K^+$, $Na^+$, $Ca^{2+}$, and $Mg^{2+}$) in $PM_{2.5}$ were measured with a 60-min time resolution during the campaign using an Ambient Ion Monitor (AIM; URG 9000D Series, USA). Detailed description of performance evaluation of AIM-IC system can be found in Malaguti et al. (2015) and Xu et al. (2017). Briefly, ambient air was introduced into the AIM with a 2-m Teflon coated aluminum pipe and particles larger than 2.5 μm were removed by a cyclone at a flow rate of 3 L/min with standard derivation of <1%. This flow rate was checked weekly with a certified flow meter. The interfering acidic and basic gases to the measurement of particle components were removed by a liquid diffusion denuder combined with a Steam-Jet Aerosol Collector followed by an Aerosol Sample Collector, until the particles can be injected into the ion chromatograph (Hu et al., 2014). The limit of detection of AIM-IC was 0.08 μg/m$^3$ for $NH_4^+$ and 0.1 μg/m$^3$ for the other ions. The multipoint calibrations were performed weekly by using standard solutions. Good linearity of ion concentrations was obtained with an $R^2$ of ≥0.99.

Ambient $NH_3$ was measured using an economical ammonia analyzer (DLT-100, Los Gatos Research LGR, USA), which utilize a unique laser absorption technology called off-axis integrated cavity output spectroscopy. Before measurement, the $NH_3$ analyzer was calibrated using a $NH_3$ permeation tube (code D145 serial n. 16570, Fine Metrology S.r.l.s., Italy) in lab. Additional description of the performance of the LGR $NH_3$ analyzer can be found in Meng et al. (2018). In brief, the analyzer has a precision of 0.2 ppb at 1-s average and a maximum drift of 0.2 ppb over 24 hr. During the campaign, $NH_3$ data were recorded as 100-s average.

Gas phase $HNO_3$ and HCl were measured by an In situ Gas and Aerosol Compositions Monitor (IGAC, Fortelice International Co., Taiwan), and hourly data were collected. Detailed description on IGAC analysis can be found in Liu et al. (2017). Besides, a set of commercial instruments were used to measure $NO_2$ (T500U CAPS, Teledyne API), $NO_y$ (TE 42CY, Thermo Environmental Instruments, Inc.), and $SO_2$ (TE 43CTL, Thermo Environmental Instruments, Inc.). Zero and span checks were performed weekly on these analyzers to identify possible analyzer malfunctions and drifts. Multipoint calibrations were performed on the instruments before and after the campaign, respectively. Measurement records were saved as 1-min averages. After the correction of data on the basis of the multipoint calibrations, hourly average data were calculated and used for this study.

The meteorological parameters, including wind speed, wind direction, relative humidity (RH), solar radiation (SR), precipitation, and temperature (T), were obtained from an automatic meteorological observation station in AOTI Park, which is a network station of meteorological observation governed by China Meteorological Administration (CMA) and nearby the IAP site (about 3 km).

### 2.3. Calculated Aerosol Acidity (pH) and Aerosol Water Content (AWC)

Different behaviors between in situ acidity and strong acidity were discussed in previous studies (He et al., 2012; Pathak et al., 2009; Zhang et al., 2007), with in situ acidity representing the acidity at the concentration of free $H^+$ (denoted by $[H^+]_{free}$ in following) or pH in the deliquesced particles at the ambient condition and strong acidity representing the acidity at the measured concentration of $H^+$ in aerosol solution. In this study, both quantities are used to investigate the variations of the aerosol acidity under different conditions. Strong acidity ($[H^+]_{SA}$) has been measured by ACSA as mentioned in section 2.2. The in situ acidity was calculated by ISORROPIA II model (http://isorropia.eas.gatech.edu), which computes the equilibrium compositions for the $Na^+$-$K^+$-$Ca^{2+}$-$Mg^{2+}$-$NH_4^+$- $SO_4^{2-}$-$NO_3^-$-$Cl^-$-$H_2O$ aerosol system (Fountoukis & Nenes, 2007). The model was run in "forward" mode to obtain the gas–particle equilibrium partitioning concentrations based on the input of total concentration of species (i.e., gas+particle). The "forward" mode can make better predictions compared with the "reversed" mode. The forward mode can solve the total (gas + aerosol) concentration of each species, while the reverse mode only use the concentration of each species in the aerosol phase as input. Besides, the particle was assumed as "metastable" with no solid participating. This assumption is reasonable since high RH often observed during the campaign. According to Guo et al. (2017), only RH range in 20–95% data was considered in computing ISORROPIA model, and the large pH uncertainty

would be introduced out of this range. The bulk particle pH was calculated using the following equation (equation (1)):

$$\mathrm{pH} = -\log_{10}\frac{1000\times\left[H^{+}_{\mathrm{air}}\right]}{\mathrm{AWC}} \quad (1)$$

where $H^{+}_{\mathrm{air}}$ ($\mu g/m^3$) is the equilibrium particle hydronium ion concentration per volume air output from ISORROPIA II model. The AWC ($\mu g/m^3$) is the aerosol water content, another output of ISORROPIA model, which was evaluated in previous studies and shows a good performance compared with particle water measurements (Bian et al., 2014; *H* Guo et al., 2015). In this study, both the measured (AWC_ACSA) and the predicted AWC (AWC_ISO) values were used to make a comprehensive analysis of the variation of the aerosol water content during pollution formation.

### 2.4. Definition of Excess $NH_x$

According to Huo et al. (2015) and Meng et al. (2011), high gas-phase $NH_3$ mixing ratios are always found in the NCP. Previous studies distinguished between $NH_3$-rich and $NH_3$-poor conditions based on the particulate ammonium-to-sulfate molar ratio ($[NH_4^+]/[SO_4^{2-}]$) being larger or smaller than 1.5 (*K* He et al., 2012; Pathak et al., 2009). In this study, similar to that reported in Liu et al. (2017), the quantity "excess $NH_x$" ($ExcessNH_x$) is introduced to examine the effect of $NH_3$ on SIAs formations as well as the fine particles pollution under different conditions (i.e., clean period and polluted period). The excess $NH_x$ is expressed as follows:

$$\mathrm{ExcessNH}_x = \frac{\mathrm{NH}_{x\text{-}\mathrm{Total}}-\left(\sum \mathrm{C}_{\mathrm{i\_anions}}-\sum \mathrm{C}_{\mathrm{i\_cations}}\right)}{\mathrm{NH}_{x\_\mathrm{Total}}}\times 100\% \quad (2)$$

where, $\sum C_i\_cations$ represents the total measured nonvolatile cations (excluding $NH_x$) needed to be equivalent with all anions ($\sum C_i$_anions) in equivalent concentration of hydrogen ion (e.g., for 1 $\mu$mol/L $SO_4^{2-}$ = 2 $\mu$eq/L $H^+$). *$NH_x$_Total* is the total ammonia, that is, gas phase $NH_3$ + particle $NH_4^+$.

### 2.5. Setup of NAQPMS Model

The Nested Air Quality Prediction Monitor System (NAQPMS; *Z* Wang et al., 2001) was applied to simulate the fine particles and the related species with a horizontal resolution of 45 km over East Asia and 20 vertical layers in a sigma coordinate during APHH-Beijing. The advection algorithm as well as the diffusion processes in NAQPMS are based on Walcek and Aleksic (1998) and Byun and Dennis (1995), respectively. The dry deposition for gas and aerosols was developed by Wesely (1989) and Zhang et al. (2001). The aqueous chemistry and wet deposition schemes are the same as used in the Regional Acid Deposition Model (RADM) (Stockwell et al., 1990) mechanism, which was used in CMAQ v4.6 and NAQPMS (*B Z* Ge et al., 2014). The gaseous chemical mechanism (CBM-Z) with additional dimethyl sulfide reactions was used including 71 species and 134 chemical reactions (Zaveri & Peters, 1999). The thermodynamic equilibrium processes of inorganic aerosols were simulated with the ISORROPIA v1.7 (Nenes et al., 1998) model using an ammonia-sulfate-nitrate-chloride-sodium-water system. Six secondary organic aerosols were processed by a two-product module (Odum et al., 1997). The simulation of heterogeneous chemical processes involved 14 chemical compounds and 28 reactions on the surface of dust, sea salt, sulfate, and black carbon particles (*J* Li et al., 2012). More detailed descriptions can be found in Wang et al. (2001) and Li et al. (2012).

The data of anthropogenic emissions (e.g., $SO_2$, $NO_x$, $NH_3$, CO, BC, OC, and volatile organic compounds) were from the MEIC inventory for China with a base year of 2016 (Zheng et al., 2018) and MIX inventory for other countries with a base year of 2010 (*M* Li et al., 2017). The biogenic emission was based on the Model of Emissions of Gases and Aerosols from Nature (MEGAN v2.0; Guenther et al., 2006), while the biomass burning emissions were from the Global Fire Emissions Database version 2 (GFEDv2; van der Werf et al., 2006). Dust emissions were computed online using the same equations as those described in Li et al. (2012). Sea salt emissions were calculated following Athanasopoulou et al. (2008). Both dust and sea salt emissions were divided into 4 size bins ranging from 0.43 to 10 $\mu$m.

The initial and lateral boundary conditions of NAQPMS were obtained from the global chemistry transport model MOZART-v2.4 (Hauglustaine et al., 1998). The meteorological field as an input of NAQPMS was

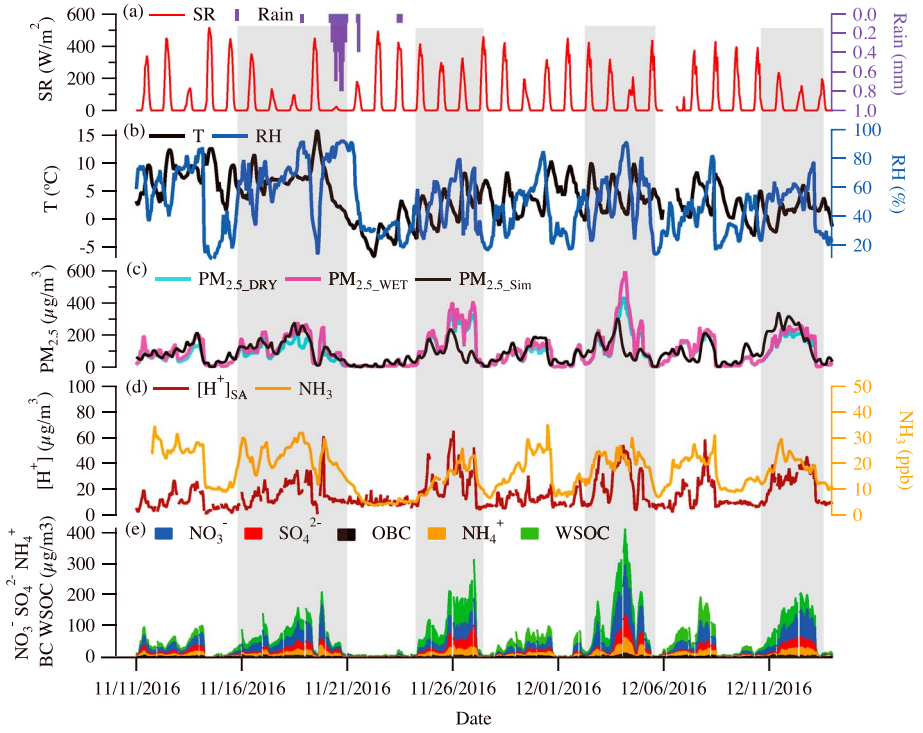


**Figure 1.** (a) Time series of solar radiation and rainfall, (b) air temperature and relative humidity (RH), (c) hourly concentrations of dry and wet particulate matter $PM_{2.5}$ as well as the simulated $PM_{2.5}$ by Nested Air Quality Prediction Monitor System (NAQPMS), (d) measured $[H^+]$ by ACSA and $NH_3$ by Los Gatos Research (LGR), and (e) chemical components of fine particles.

provided by the Weather Research and Forecasting model (WRF; ver. 3.7.1, http://www.wrf-model.org) using the same domain and horizontal resolution. The boundary and initial conditions of the WRF were based on final analysis (FNL) data from the National Centers for Environmental Prediction (NCEP) in the United States. The simulation period is from November to December of 2016 with 1 week of spin up before the observation period of APHH-Beijing winter campaign. The NAQPMS with the above settings has been used successfully to simulate the temporal and spatial variation of $PM_{2.5}$ and $PM_{10}$, as well as their inorganic components over Beijing and East Asia, and shown similar performances as the CMAQ and Goddard Earth Observing System-Chemistry (GEOS-Chem) model (Uno et al., 2017; Wang, Itahashi, et al., 2017; Wang et al., 2018; Wang, Pan, et al., 2017).

## 3. Results and Discussion

### 3.1. Temporal Variations

#### 3.1.1. Time Series

Figure 1 shows the temporal variations in hourly concentration of $NO_3^-$, $SO_4^{2-}$, $NH_4^+$, optical black carbon, water soluble organic carbon, $[H^+]_{SA}$, $NH_3$, measured dry and wet $PM_{2.5}$, and simulated $PM_{2.5}$. Meteorological parameters, such as ambient temperature (T), RH, SR, and accumulative precipitation, are also plotted on the figure. During the observation period, there were four heavy pollution events (15–18 and 25–26 November and 3–4 and 11–12 December) according to the daily averaged concentration of China National Ambient Air Quality Standards (CNAAQS, $PM_{2.5}$>150 μg/m$^3$). The highest concentrations of hourly dry and wet $PM_{2.5}$ reached 438 and 633 μg/m$^3$, respectively. The levels of SIAs (e.g., $SO_4^{2-}$, $NO_3^-$, and $NH_4^+$) were significantly elevated during the polluted periods compared with the nonpolluted periods, with the total fraction of these three components increasing from 28 to 48%. The concentrations of dry and wet $PM_{2.5}$ were quite close to each other during non-polluted periods but showed substantial differences during polluted periods. As mentioned in section 2.3, the difference of dry and wet $PM_{2.5}$ is recognized as AWC. Details of AWC and its driving factors will be discussed in section 3.3. The mass concentration of

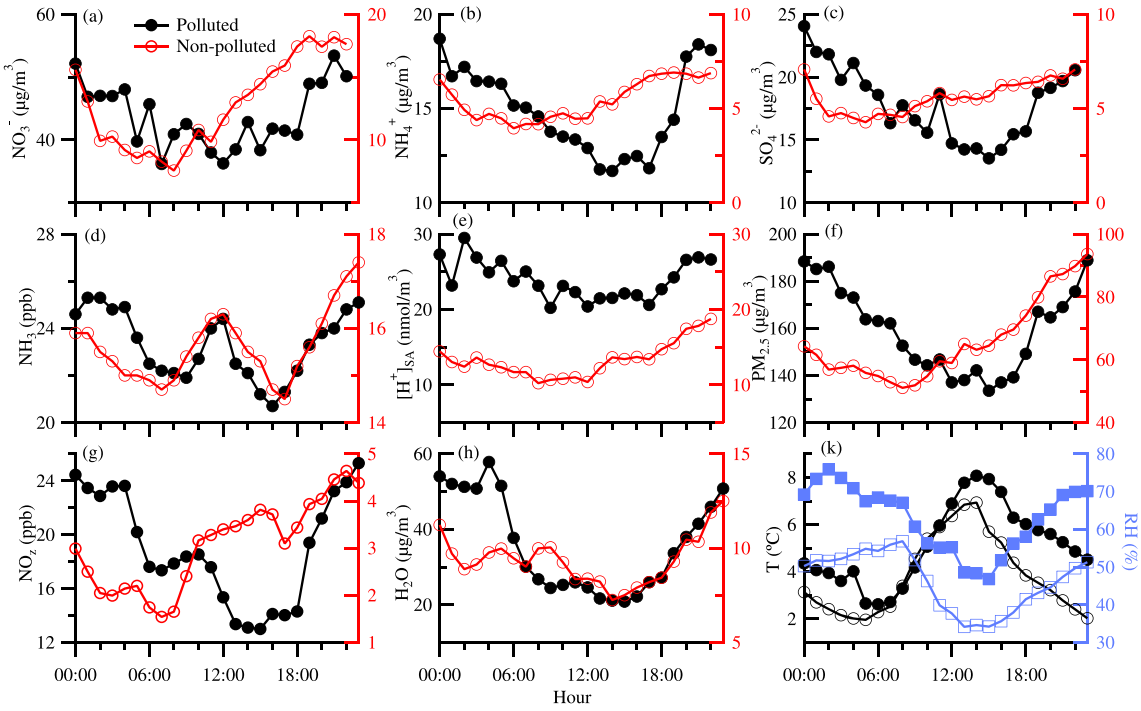


**Figure 2.** Diurnal cycles of particle (a) $NO_3^-$, (b) $NH_4^+$, (c) $SO_4^{2-}$, (d) gaseous $NH_3$, (e) $[H^+]_{SA}$, (f) $PM_{2.5}$, (g) gaseous $NO_z$, (h) AWC, (k) temperature and relative humidity in polluted (line with solid circles/squares), and nonpolluted (line with hollow circles/squares) periods.

$PM_{2.5}$ simulated by NAQPMS followed the trends of measured $PM_{2.5}$ for most of the time but showed large deviations from that of measured $PM_{2.5}$ sometimes during the polluted periods.

### 3.1.2. Diurnal Variations Under Different Pollution Conditions

Figure 2 shows the average diurnal cycles of concentrations of inorganic aerosols, $NH_3$, $NO_z$ (≡$NO_y$-$NO_x$), $[H^+]_{SA}$, AWC, and $PM_{2.5}$ as well as the meteorological parameters (T and RH) for the polluted and nonpolluted conditions. Under nonpolluted conditions, nitrate shows a clear daytime increase starting from ~9:00 LT and reaching a maximum at ~19:00 LT. Since nonpolluted conditions corresponded to lower RH (Figure 2k) and higher SR (Figure S1 in the supporting information) during the daytime, photochemical production should be the major driver of the observed daytime increase in nitrate. The nitrate production rate during the daytime was ~1 μg/m$^3$/hr, a little higher than that reported in the whole winter of 2011 (0.6–0.8 μg/m$^3$/hr) by Sun et al. (2015). Under polluted conditions, the nitrate concentration was 2–3 times higher than those under nonpolluted conditions and showed a maximum around midnight and a broad valley during the daytime. In this case, the relative contribution of the daytime photochemical production to the formation of $NO_3^-$ may be significantly reduced under the weak radiation (Figure S1). The production of $NO_3^-$ from $N_2O_5$ heterogeneous reactions during the nighttime of polluted periods should be much more important than that in nonpolluted periods, as higher $N_2O_5$ level and RH favored the heterogeneous formation of $NO_3^-$. Daytime $NO_z$ showed an increasing trend under nonpolluted condition and a decreasing trend under polluted condition (Figure 2g). This phenomenon also indicates a more important photochemical contribution in nonpolluted periods since $NO_z$ is the sum of the photochemical products from $NO_x$ reactions. $HNO_3$ is the major component of $NO_z$, with an average contribution 48.8% to $NO_z$ during the most polluted period of the campaign (Figure S2). The decreasing trend of $NO_z$ in daytime under polluted conditions suggests that the photochemical production of $NO_z$ cannot compensate the loss caused by dry deposition and aerosol uptake as well as the dilution effects driving by the planetary boundary layer (PBL) height elevation. It has been proved that the PBL height is higher in the daytime especially around noon to afternoon than that in the nighttime even in the heavy polluted conditions (Tang et al., 2016; Xiang et al., 2019). During our observation, CO also showed a clear daytime valley even under the polluted condition (Figure S3) though CO can be considered as a relatively inert gas. This confirms that the PBL elevation during the daytime did play a role in lowering the $NO_z$ concentration. Dry deposition and aerosol uptake may efficiently

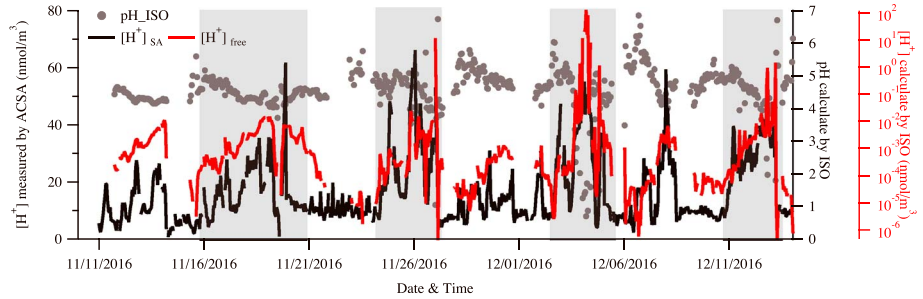


**Figure 3.** Time series of calculated aerosol pH (in grey solid point) and free $[H^+]_{free}$ concentration (in red line) by ISORROPIA II as well as the measured strong acidity $[H^+]_{SA}$ (in black line) by ACSA during the campaign.

remove $NO_z$ during the daytime and nighttime, particularly under the polluted condition. However, the high nighttime $NO_z$ were sustained in the polluted case probably by rapid formation of $NO_z$ through the $N_2O_5$ pathway and depressed PBL height. During the daytime, the photochemical production of $NO_z$ was weakened due to reduced radiation under haze pollution so that the $NO_z$ level was lowered under the combined effect of dry deposition, aerosol uptake, and the elevated PBL height.

Relatively small diurnal variations were observed for sulfate and ammonium in nonpolluted case, with only a slight increase during 08:00–22:00 LT. The average daily amplitude of the $NO_3^-$ concentration (10 μg/m$^3$) is much higher than that of $SO_4^{2-}$ (2.8 μg/m$^3$). This suggests that either the daytime photochemical production of sulfate is low or it is masked by the changes in the PBL height. If the later was true, the $NO_3^-$ concentration would have been impacted as well. Sun et al. (2015) reported the diurnal variations of sulfate in $PM_1$ at the same site during four seasons and pointed out that the daytime photochemical production of sulfate is more distinct in May, June, and October but less pronounced in winter. Therefore, the smaller amplitude of $SO_4^{2-}$ should be due to lower photochemical conversion of $SO_2$ under nonpolluted winter condition. In contrast to the nonpolluted condition, significant variations in $SO_4^{2-}$ and $NH_4^+$ were observed when it was severely polluted, with a decreasing trend from the midnight to late afternoon and a rapid increase afterwards. As a result, the diurnal variations of $PM_{2.5}$ are significant different for polluted and nonpolluted cases with nearly reversed daytime trends. In other words, the photochemical production may not be the factor dominating the diurnal cycle of fine particle pollution during winter polluted cases in Beijing.

The diurnal variations of $NH_3$ in polluted periods were similar as that in nonpolluted periods and showed a maximum around midnight and a broad valley during the daytime except the peaks around noon (Figure 2d). However, these diurnal variations were not consistent well with that observed in a rural site of NCP during summer by Meng et al. (2018), who observed the maximum concentrations during the daytime (09:00–13:00). Higher agricultural emission of $NH_3$ in rural area and potential evaporation of $NH_3$ from particles under high temperature in summer may explain the high values of $NH_3$ in the daytime. Both of our study and the June–September observation at the rural site by Meng et al. (2018) show a decreasing trend of $NH_3$ from 13:00 to 18:00. Besides the conversion of $NH_3$ to $NH_4^+$, dry deposition may be a key factor in the decrease of $NH_3$ concentration. Pan et al. (2018) compared the dry deposition flux of $NH_3$ with the gridded emission from MEIC (http://meicmodel.org) and showed that the dry deposition flux would took up almost 1/3 emission in Beijing (10-15 kg N · ha$^{-1}$ · year$^{-1}$ for dry deposition flux and 30–40 kg N · ha$^{-1}$ · year$^{-1}$ for the emission) and 1/2 in farmland of surrounding Beijing (20–25 kg N · ha$^{-1}$ · year$^{-1}$ for dry deposition flux and 40 kg N · ha$^{-1}$ · year$^{-1}$ for the emission).

### 3.2. Acidity of Aerosols and Its Relations With the Haze Pollution

Figure 3 shows the measured strong acidity $[H^+]_{SA}$ and the calculated free $[H^+]_{free}$ as well as pH value (pH_ISO). $[H^+]_{SA}$ and $[H^+]_{free}$ show much higher concentrations under polluted than nonpolluted conditions. The pH value calculated using equation (1) varies in the range of 0.7–6.8 with a median of 4.6 for the whole period, indicating a medium acidic condition for fine particles during haze pollution in the winter of Beijing. This suggests that the aerosol particles at our site in winter are less acid compared with those at some other sites. For example, Guo et al. (2017) reported the bulk pH of $PM_{2.5}$ during 2010 California

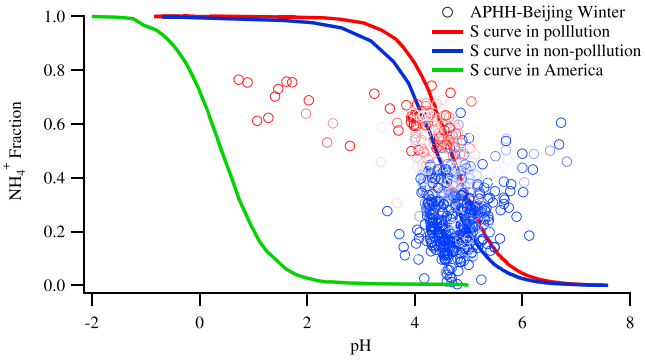


**Figure 4.** Analytically calculated *S* curves of the fraction of $NH_x$ (gas $NH_3$ + particle $NH_4^+$) in the particle phase and ambient data, plotted with ISORROPIA II-predicted pH for APHH-Beijing winter Campaign. The red and blue lines are calculated based on the averaged ambient data in polluted and nonpolluted conditions of APHH-Beijing, while the green line is based on the data reported in California by Guo et al. (2017).

Research at the Nexus of Air Quality and Climate Change (CalNex) campaign as more acidic particles (mean value of 2.7±0.3). Bougiatioti et al. (2016) also found more strong aerosol acidity in the European supersite located in Greece ranging from −1.0 to 3.8 during August–November. It is noted that the concentration of $NH_3$ during our observations was much higher (17.1 ppb on average) compared to those (lower than 5 ppb) observed in Europe and North America. The higher pH value in Beijing is attributable to higher concentrations of $NH_3$. Liu et al. (2017) also reported a similar pH range (3.0–4.9) during the winter haze pollution in Beijing. This medium aerosol acidity resulted in the partition of $HNO_3$ predominately into particle phase, with the fraction of $NO_3^-$ reaching 90% (Yue et al., 2013). In contrast, the fraction of $NO_3^-$ during CalNex campaign (Ryerson et al., 2013) in North America was only 60% under pH value varied in 2–3 conditions (Guo et al., 2017). This is consistent with the findings by Guo et al. (2017), who showed a "S" curve dependence of the partition of $HNO_3$ on the pH of particles with low value of pH corresponding to the low fraction of aerosol $NO_3^-$. It should be noted that Guo et al. (2017) also find that there is almost no fraction of $NH_4^+$ under the medium acidity (pH>3) condition. However, the fraction of $NH_4^+$ in this study is 46% and 32% for polluted and nonpolluted conditions with the median particle pH being 3.6 and 4.5 (as shown in Figure 4), respectively. This indicates that the relationship between the bulk pH of particles and the partitioning of $NH_3$ in Beijing is very different from that in California, with the later showing $NH_3/NH_4^+$ partitioning effects in lower range of pH. The cause will be investigated in the following section.

### 3.3. Impacts of Excess $NH_x$ on Aerosol Acidity and AWC

To examine the effects of the ammonia on aerosol acidity and AWC, we define excess $NH_x$ (equation (2)), which represents the remaining fraction of $NH_x$ after subtracting $NH_x$ needed to balance the portion of total observed anions that cannot be balanced by observed metal ions or cations other than $NH_4^+$ and $H^+$. Figure 5 shows the time series of excess $NH_x$, $PM_{2.5}$, and AWC measured by ACSA ($AWC_{\_ACSA}$) and calculated using ISORROPIA II ($AWC_{\_ISO}$). The measured AWC is highly correlated with the calculated AWC

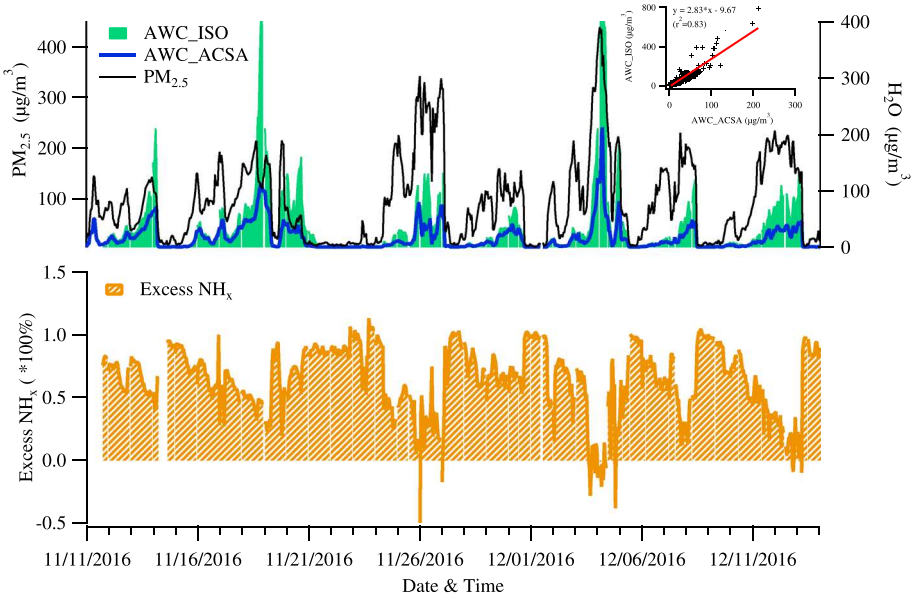


**Figure 5.** Comparison of measured aerosol water content (AWC) by ACSA (in blue line), calculated by ISORROPIA II (in green solid column) and (a) the concentration of $PM_{2.5}$ (in black line) and (b) the time series of Excess $NH_x$ during the campaign.

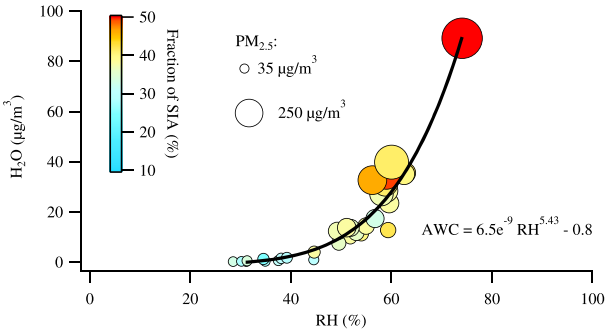


**Figure 6.** Aerosol water content as a function of relative humidity (RH) with respect to the inorganic fraction in particulate matter $PM_{2.5}$ (SIA %) as well as the $PM_{2.5}$ mass concentration. The circles are colored according to the secondary inorganic aerosol (SIA) fraction and the sizes of the circles are scaled to the $PM_{2.5}$ mass concentration.

($R^2$>0.8, see the subplot in Figure 5), indicating that both the measurement and simulation captured the variations of AWC during the observation period. It can be seen in Figure 5 that higher AWC corresponds to higher concentration of $PM_{2.5}$ ($r^2$=0.54, $p$<0.01). This suggests that AWC plays an important role in the increase of the $PM_{2.5}$ level. Wu et al. (2018) reported a positive feedback loop between the elevated AWC due to high RH levels and the increasing of aerosol mass as well as the water-soluble inorganic fractions. They proposed that there exist a driving force for gaseous pollutants, such as $SO_2$ and $NO_x$, for the transformation of particulate SIAs ($SO_4^-$, $NO_3^-$, and $NH_4^+$). Under the Henry's law equilibrium, the particles with high AWC would take up more gaseous pollutants and prepared for the chemical reaction to occur, while the thermodynamic equilibrium lead to increase their water and inorganic contents to ensure the aqueous solution water activity remains equal to the RH. This mechanism enhances the SIA fraction and AWC under heavy haze pollution. In this study, we also observed a significant positive correlation between RH and SIAs fraction as well as the $PM_{2.5}$ concentration (Figure 6).

Excess $NH_x$, however, shows an opposite relationship with $PM_{2.5}$ and AWC (Figure 5), clearly indicating more conversion of $NH_3$ to particle $NH_4^+$ under higher AWC condition and hence contributing to the increase in the high concentration of $PM_{2.5}$ during the winter haze pollution. Further evidence is provided by the scatter plot of aerosol acidity versus excess $NH_x$ in Figure 7. As shown in this figure, the pH value of fine particles increases significantly with the increase of excess $NH_x$, especially under polluted conditions. Less excess $NH_x$ is related to more portion of $NH_4^+$ in particles, which is used to neutralize the anions ($SO_4^{2-}$ and $NO_3^-$, etc) in $PM_{2.5}$. A few low-pH points are associated with negative excess $NH_x$, meaning that the $NH_3$ levels were too low to neutralize the produced acids. However, these cases occurred only very infrequently. As we know, at least part of $(NH_4)_2SO_4$ and $NH_4NO_3$ will hydrolyze under the existence of AWC and produce $H^+$ so that fine aerosol particles become acidic. The $NH_x$ enters into the equilibrium system of $H_2SO_4$-$HNO_3$-$H_2O$ and produces more portion of $NH_4^+$, which may prevent the dissociation of $H^+$ from the system and hence to neutralize the particles acidity. This makes the negative correlation between the aerosol acidity and excess $NH_x$. Moreover, the pH of aerosols shows a logarithmic relationship with the amount of excess $NH_x$, and finally, the increasing trend of aerosol pH becomes insensitive to the excess $NH_x$. This is consistence with that reported in previous studies (Bougiatioti et al., 2016; Liu et al., 2017; Weber et al., 2016) and contradictory to the result in Wang et al. (2016), who stated that the ambient $NH_3$ could completely neutralize fine particles (pH≈7) during haze pollution in northern China.

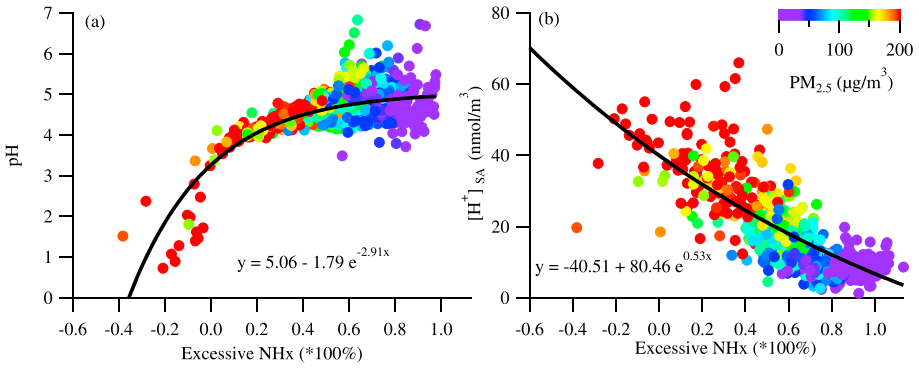


**Figure 7.** Impacts of Excess $NH_x$ on fine particle pH. Relationship between predicted pH and Excess $NH_x$ (a). Relationship between measured [$H^+$] by ACSA and Excess $NH_x$ (b) with colored at different level of $PM_{2.5}$ concentrations.

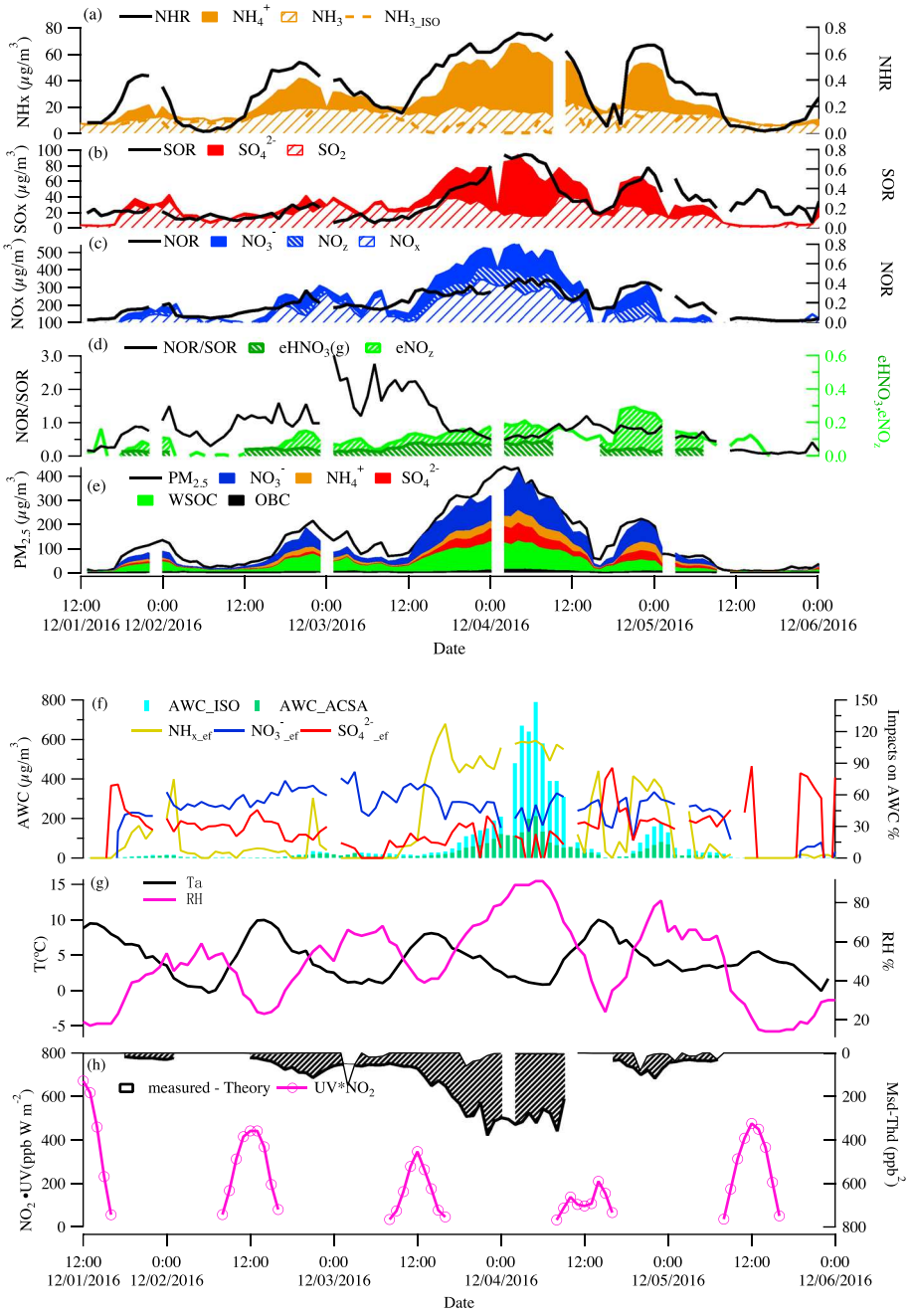


**Figure 8.** (a) Time series of measured gaseous $NH_3$, particle $NH_4^+$ and the ratio of $NH_4^+/(NH_3+NH_4^+)$ NHR as well as the $NH_3$ simulated by ISORROPIA II model in dashed line; (b) $SO_2$, particle $SO_4^{2-}$, and the ratio of $SO_4^{2-}/(SO_2+ SO_4^{2-})$ SOR; (c) $NO_x$, particle $NO_3^-$, and the ratio of $NO_3^-/(NO_2+ NO_3^-)$ NOR; (d) ratio of NOR/SOR, ratio of $HNO_3$, and $NO_z$ in total $NO_y$, and (e) the $PM_{2.5}$concentration as well as its components fraction for $NO_3^-$, $SO_4^{2-}$, $NH_4^+$, water soluble organic carbon (WSOC), and optical black carbon (OBC).Time series of the measured aerosol water content (AWC) in green bar and calculated AWC in light blue bar as well as the three inputs ($NH_{x\_ef}$ is the ammonium effects, similar with $SO_4^{2-}{}_{ef}$ and $NO_3^-{}_{ef}$) effects to the (f) AWC, (g) relative humidity (RH) and air temperature, and (h) $NO_2$×UV, a surrogate of photochemical production rate of $HNO_3$ in the daytime as well as the measured and theoretical calculated products of the partial pressure of $NH_3$ and $HNO_3$ represents the thermodynamic equilibrium ability for $NH_4NO_3$.

### 3.4. Role of Ammonia in the Formation of Heavy Pollution

As is mentioned above, there were four major pollution events during the whole campaign. The heaviest pollution was the one during the 3–4 December 2016 (Figure 8), with the daily averaged $PM_{2.5}$ concentration

(262 μg/m$^3$ on 4 December) over the threshold of the serious level according to the CNAAQS (24-hr averaged concentrations $PM_{2.5}$>250 μg/m$^3$). To investigate the role of ammonia in the formation of heavy pollution, we focus on the variations of major inorganic components in $PM_{2.5}$ and their precursors as well as some key related parameters in, before, and after this heavy pollution episode. We calculated oxidation ratios of $SO_2$ (SOR: $nSO_4^{2-}/(nSO_4^{2-}+nSO_2)$) and $NO_2$ (NOR: $nNO_3^-/(nNO_3^-+nNO_2)$) as well as the conversion ratio of $NH_3$ (NHR: $nNH_4^+/(nNH_4^++nNH_3)$). These ratios are present in Figures 8a–8c, together with the concentrations of related precursors and products. To see the relative changes of NOR and SOR during the process, the ratio NOR/SOR was calculated and shown in Figure 8d, along with the observed ratios of $NO_z$ ($eNO_z$) and $HNO_3$ ($eHNO_3$) to total $NO_y$ (gaseous $NO_y$ + particle $NO_3^-$). The variations of $PM_{2.5}$ and its major components are displayed in Figure 8e. On average, the sum of SIAs contributed to almost 57% of $PM_{2.5}$ during this event, with $SO_4^{2-}$, $NO_3^-$ and $NH_4^+$ accounting for 11%, 33%, and 13%, respectively. These contributions were even higher during the nighttime. NHR, SOR, and NOR increased from 1 to 75%, from 7 to 75%, and from 4 to 45% (Figures 8a–8c), respectively. Although NOR was much lower than SOR and NHR during the pollution period, the mass contribution of nitrate to $PM_{2.5}$ was the largest (33%) among the SIAs (Figure 8e). This is mainly due to the higher $NO_x$ level compared to those of $SO_2$ and $NH_3$.

In order to investigate the transform pathway of $NO_x$, the photochemical production rate of $HNO_3$ using $NO_2 \times UV$ as a surrogate during the daytime (Ge et al., 2013; Sun et al., 2011) and the stability of $NH_4NO_3$ expressed by the difference in the observational and theoretical product of the partial pressure of $NH_3$ and $HNO_3$ (Hao et al., 2017) have been employed and shown in Figure 8h. The main chemical reaction equations of the transformation of $NO_x$ to $NO_3^-$ are listed below ((R1)-(R6)):

(R1) $$NO_2 + OH + M \rightarrow HNO_3 + M$$

(R2) $$NO_2 + O_3 \rightarrow NO_3 + O_2$$

(R3) $$NO_2 + NO_3 + M \leftrightarrow N_2O_5 + M$$

(R4) $$N_2O_5 + H_2O(aq) \rightarrow 2\ HNO_3$$

(R5) $$HNO_3(g) + NH_3(g) \leftrightarrow NH_4NO_3\ (s) \quad (RH<DRH)$$

(R6) $$HNO_3(g) + NH_3(g) \leftrightarrow NH_4^+(aq) + NO_3^-\ (aq) \quad (RH>DRH)$$

Generally, $NO_2$ is oxidized to $HNO_3$ via reaction with OH (R1) that is mainly photochemically produced in the daytime and heterogeneous reactions ((R2)-(R4)) that occur mainly in the nighttime. After the production of $HNO_3$, the gas-particle equilibrium reaction among $HNO_3$, $NH_3$, and $NH_4NO_3$ determines the concentration of $NH_4NO_3$ aerosol, with its phase depending on RH conditions (R5–R6).

Higher RH promotes the hygroscopic growth of aerosol particles, particularly those containing significant amount of $NH_4NO_3$. Deliquescence of aerosol occurs at RH equal to and greater than its deliquescence relative humidity (DRH). Over a continental site like IAP, $NH_4NO_3$, $(NH_4)_2SO_4$, and $NH_4Cl$ are usually the main components of SIA under ammonia-rich conditions as in our case (Figure 5). Among these components, $NH_4NO_3$ has the lowest DRH (62% at 25°C, 77% at 0°C; Seinfeld & Pandis, 2006). The air temperature in our pollution case varied in the range of 0–10°C. Therefore, deliquescence of pure $NH_4NO_3$ would occur at RH from 70.5 to 76.6%. Since $NH_4NO_3$ was the major salt in aerosol particles and mixed with $(NH_4)_2SO_4$, $NH_4Cl$, etc., particle deliquescence should occur at RH significantly lower than the DRH of $NH_4NO_3$. Calculated molar ratio $(NH_4)_2SO_4/[(NH_4)_2SO_4+NH_4NO_3]$ varies in the range of 0.05–0.29 for the period 1–4 December. Suppose water activity of aerosol was controlled by the $(NH_4)_2SO_4+NH_4NO_3$ mixture, the DRH point would be about in the range of 50–60%, as estimated using the molar ratio $(NH_4)_2SO_4/[(NH_4)_2SO_4+NH_4NO_3]$ and data in Seinfeld and Pandis (2006). The DRH for the mixed system of the $(NH_4)_2SO_4$, $NH_4NO_3$, and $NH_4Cl$ was 46% as estimated using the ISORROPIA II model. Indeed, deliquescence took place during the two nights (2 and 3 December) prior to the heavy pollution, when RH was about 50–65% (Figure 8g). The humidity conditions, particularly during the daytime, inhibited further hygroscopic growth of aerosols during the time prior to heavy pollution. Nevertheless, aerosol particles became wet as indicated by the AWC data in Figure 8f and were nearly ready for enhanced heterogeneous reactions. After the noon time of 3 December RH increased rapidly and reached around 80% at about 0:00 LT on 4

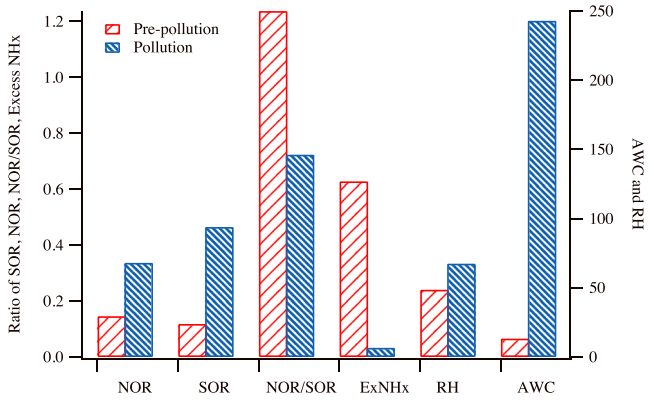


**Figure 9.** Comparison of SOR, NOR, NOR/SOR, excess $NH_x$, relative humidity (RH) and aerosol water content (AWC) between the pre-pollution stage (0:00 2 December to 13:00 3 December) and pollution stage (14:00 3 December to 14:00 4 December) during episode 2–4 December 2016.

December, much higher than the DRH point. Such high RH condition favored the reaction of R6, as reflected by the substantially enhanced measured minus theoretical products of partial pressures of $NH_3$ and $HNO_3$ (Figure 8h). Since the photochemical production rate of $HNO_3$ in the daytime of 3–4 December was small compared to the other days, the $HNO_3$ formation on these days should be mainly through the heterogeneous pathway (R2–R4). This is supported by the $eNO_z$ and $eHNO_3$ values, which increased from 0.07 and 0.03 at 1:00 LT on 3 December to 0.21 and 0.09 at LT 5:00 on 4 December (Figure 8d) during the nighttime, respectively. This is also consistent with that reported by He et al. (2018), who used the oxygen isotope methods to find the importance of nocturnal chemistry in nitrate production in Beijing haze.

As is mentioned in section 3.3, AWC is highly correlated with the $PM_{2.5}$ concentration, especially with the inorganic fraction in $PM_{2.5}$. During the episode as shown in Figure 8f, very high AWC occurred in the nighttime from 3 to 4 December and in the morning of 4 December. This high AWC episode coincided with the high level of $PM_{2.5}$ and its compositions. To clearly demonstrate the importance of AWC in haze formation over our site, we divided our data from 2–4 December 2016 into two groups, corresponding to a prepollution stage (0:00 2 December to 13:00 3 December) and a pollution stage (14:00 3 December to 14:00 4 December), respectively. Figure 9 displays the average values of NOR, SOR, NOR/SOR, excess $NH_x$, RH, and AWC during the prepollution versus those during the pollution stage. During the pollution stage, the value of excess $NH_x$ (0.03) was only 1/19 of that during the prepollution stage. The NOR and SOR values during the prepollution stage were 0.15 and 0.12, respectively, while the values during pollution stage became 0.34 and 0.46, respectively. These resulted in a change of NOR/SOR from 1.34 to 0.84. The ratio $SO_4^{2-}/NO_3^-$ (not shown) increased from 0.17 during the prepollution stage to 0.38 during the pollution stage, indicating a speed-up of $SO_2$ oxidation under the pollution condition. Since haze pollution usually weakens the photochemical condition, the observed speed-up of $SO_2$ oxidation must have been caused by heterogeneous conversion of $SO_2$ under very large AWC (average 243 $\mu g/m^3$). As clearly shown in Figure 9, a small increase in RH from the prepollution to pollution condition (from 49 to 67%) resulted in a 18.3-fold increase in AWC (from 13.3 to 243 $\mu g/m^3$). This large increase in AWC prepared conditions for rapid heterogeneous reactions and formation of SIAs.

As discussed above, the existence of a large fraction of $NH_4NO_3$ in $PM_{2.5}$ significantly lowered the DRH of aerosol, making the aerosol particles ready for enhanced heterogeneous reactions. RH in this pollution episode did not stop by about 65% but increased up to 82%. This humidity condition largely promoted the conversion of $SO_2$ to $SO_4^{2-}$ through heterogeneous reactions, as shown in Figure 8b. For most time from 0:00 LT on 2 December to 15:00 LT on 3 December the ratio NOR/SOR was in the range of 1.0–3.0 (Figure 8d) but dropped rapidly to less 1.0 at around 15:00 LT on 3 December and to 0.5 around midnight. The observed RH at 15:00 LT on 3 December was about 50%. Although there was no obvious increase in ambient $SO_2$, rapid $SO_2$ uptake and heterogeneous oxidation by oxidants (e.g., $HO_x$, $O_3$, Fe, and Mn) led to large formation and accumulation of sulfate in the wet aerosol particles. NOR increased slightly and stayed around 0.4, suggesting that the formation of aerosol nitrate was also promoted by humid and dark conditions. Increased productions of sulfate and nitrate consumed more and more ammonia, largely reduced excess $NH_x$ (Figure 9), and even caused an ammonia-poor condition for a short period of 3–4 December 2016 (Figure 5). Consequently, aerosol particles grew further and took up more water under the humid condition, resulting in a larger AWC. The 18.3-fold increase in AWC (from 13.3 $\mu g/m^3$ in the prepollution stage to 243 $\mu g/m^3$ in the pollution stage) can speed up the heterogeneous reactions, forming a positive feedback loop.

It is proposed that AWC plays key role in haze formation over the NCP and is driven by anthropogenic SIAs (Wu et al., 2018). However, the most important factor driving the increase of AWC under certain RH remains unclear. In this study, simulations are made using ISORROPIA II model by cutting down 50% of the three input species, that is, $NH_3/NH_4^+$, $HNO_3/NO_3^-$, and $SO_4^{2-}$, while keeping the other conditions unchanged. Impacts of $NH_3/NH_4^+$ ($NH_{x\_ef}$), $HNO_3/NO_3^-$ ($NO_3^-{}_{-ef}$), and $SO_4^{2-}$ ($SO_4^{2-}{}_{-ef}$) on AWC are

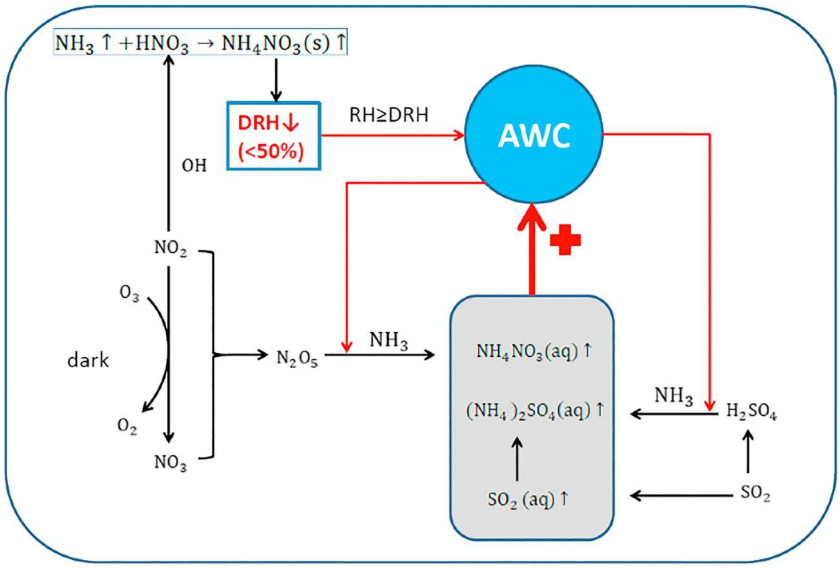


**Figure 10.** Schematic showing the role of excess $NH_x$ in the formation of heavy particulate matter $PM_{2.5}$ pollution over the North China Plain (NCP).

shown in Figure 8f. As can be seen in this figure, the effects of nitrate on AWC were higher than 60% for most of the time and is most important during the first stage of the episode (0:00 LT on 2 December to 12:00 LT on 3 December). Thereafter, the importance of ammonium effects gained a sudden enhancement and reached even over 90% during the most serious polluted stage (14:00 LT on 3 December to 12:00 LT on 4 December). The impact from sulfate on AWC was lower than 30% for most of time in the period. The results of the sensitive simulation by ISORROPIA II model indicate that $NH_4NO_3$ is the most important factor driving AWC, with $NO_3^-$ (excess $NH_x$) controlling the prior pollution stage and $NH_4^+$ (no excess $NH_x$) the most polluted stage.

In summary, excess $NH_x$ increases the formation of $NH_4NO_3$, which triggers the decrease of aerosol DRH even down to less than 50%, causes the formation of AWC through hygroscopic growth even under RH conditions lower than 50% and preconditions the aerosol particles for rapid heterogeneous reactions. A further increase of RH enlarges the positive feedback "AWC-heterogeneous reactions" and ultimately leads to the formation of severe haze. As shown in Figure 9, a small increase in average RH from 49 to 67% resulted in an increase in average AWC from 13.3 to 243 $\mu g/m^3$. This large increase in AWC caused a 9.9-, 4.4-, and 4.5-fold increase in the observed $SO_4^{2-}$, $NO_3^-$, and $NH_4^+$, respectively. Figure 10 shows schematically the role of excess $NH_x$ in the formation of heavy $PM_{2.5}$ pollution over the NCP. This may also be applicable to other regions with similar emissions and meteorological conditions.

### 3.5. Sensitivity of Fine Particle Formation to $NH_3$ Emission Change

Effects of $NH_3$ to the formation of inorganic aerosols has been further investigated using the NAQPMS model through setting up two simulations, with the one being the base case (CTL) with the normal emission and the other being the same as the CTL but with increased $NH_3$ emission (Inc$NH_3$ hereafter) by 20%. The performance of the CTL has been validated against observations in Figure S3. Overall, NAQPMS reproduced each of the polluted episodes very well during the APHH-Beijing winter campaign though it underestimated the concentrations of $PM_{2.5}$ and its inorganic components in 26–27 November and 3–4 December and overestimated those in 18–19 November as well as 11–13 December. The poor agreements during some periods may be due to the uncertainties in the meteorological simulations. Different from that reported in Gao et al. (2016), the uniform relative increase in $NH_3$ emission for each grid is chosen in this study for examining the sensitivity of formation of inorganic aerosols to the $NH_3$ perturbation. The clean period, which is defined as the concentration of $PM_{2.5}$ lower than 75$\mu g/m^3$, has been chosen instead of the nonpolluted days for comparison with the polluted case in a super-ideal manner. Figure 10 displays the impacts of $NH_3$ on the

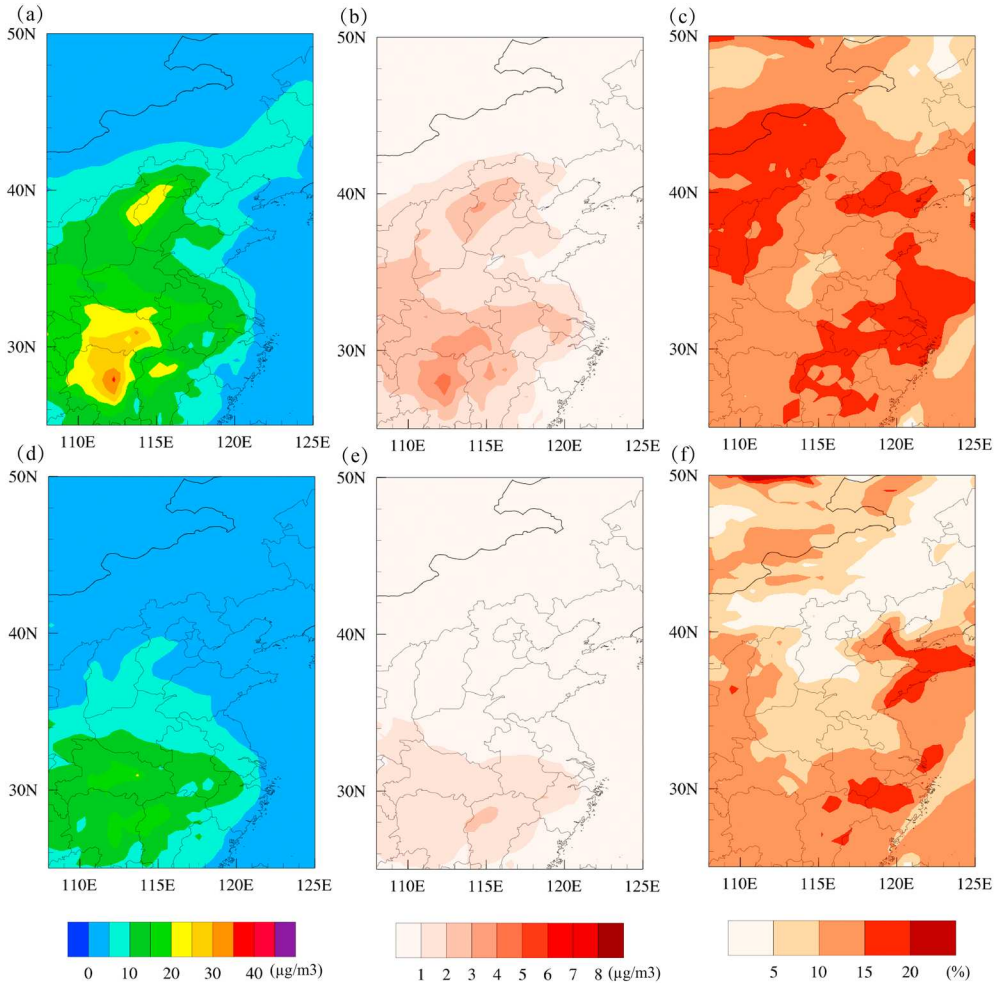


**Figure 11.** (a and d) Simulated $NH_4^+$ concentrations during polluted and nonpolluted period, (b and e) differences between the 20% increment of $NH_3$ emission scenario and the base simulations, and (c and f) the relative differences in percentage.

ammonium in particle phase during polluted and clean cases, respectively. In the polluted case, the averaged ammonium concentrations over the NCP are 10–25 $\mu g/m^3$ with the highest value reaching at 20–25 $\mu g/m^3$ mostly concentrated in the narrow belt alone with the Mt. Taihang (straight black Line in Figure 11) and Mt. Yan (straight blue Line in Figure 11) from southwest to northeast. This belt is the well-known high level of air pollution area over the NCP (Ge et al., 2012; Lin et al., 2009). During this case, 20% increase in $NH_3$ emission results in additional ammonium of 10–15% (2–4 $\mu g/m^3$) relatively to the CTL run. In the clean case, smaller changes in ammonium occur between the Inc$NH_3$ and CTL scenarios. The differences between CTL and Inc$NH_3$ scenarios imply that the ammonium formation under polluted conditions is more sensitive to increases in $NH_3$ emission than under clean conditions. However, the sensitivity changes with location. The most significant relative changes (greater than 15%) are located in the Bohai Bay and the northwest of NCP, that is, western Shanxi and middle of Mongolia, where the levels of ammonium concentrations are low, and hence, small absolute changes can result in large relative differences.

The responses of $SO_4^{2-}$ and $NO_3^-$ to the $NH_3$ emission increasing were also simulated and are displayed in Figures S4 and S5. In polluted cases, $NO_3^-$ is most sensitive to the $NH_3$ emission changes with a relative increase of 20–40% over the NCP, followed by $NH_4^+$ (10–20%) under 20% $NH_3$ emission change. For $SO_4^{2-}$, the change is the lowest compared with those of the other two inorganic aerosols, with the relative differences lower than 5%. In spite of the different simulations with that reported in Gao et al. (2016), our results multiplied by 5 times (considering the linearity response to the $NH_3$ emission) are consistent with

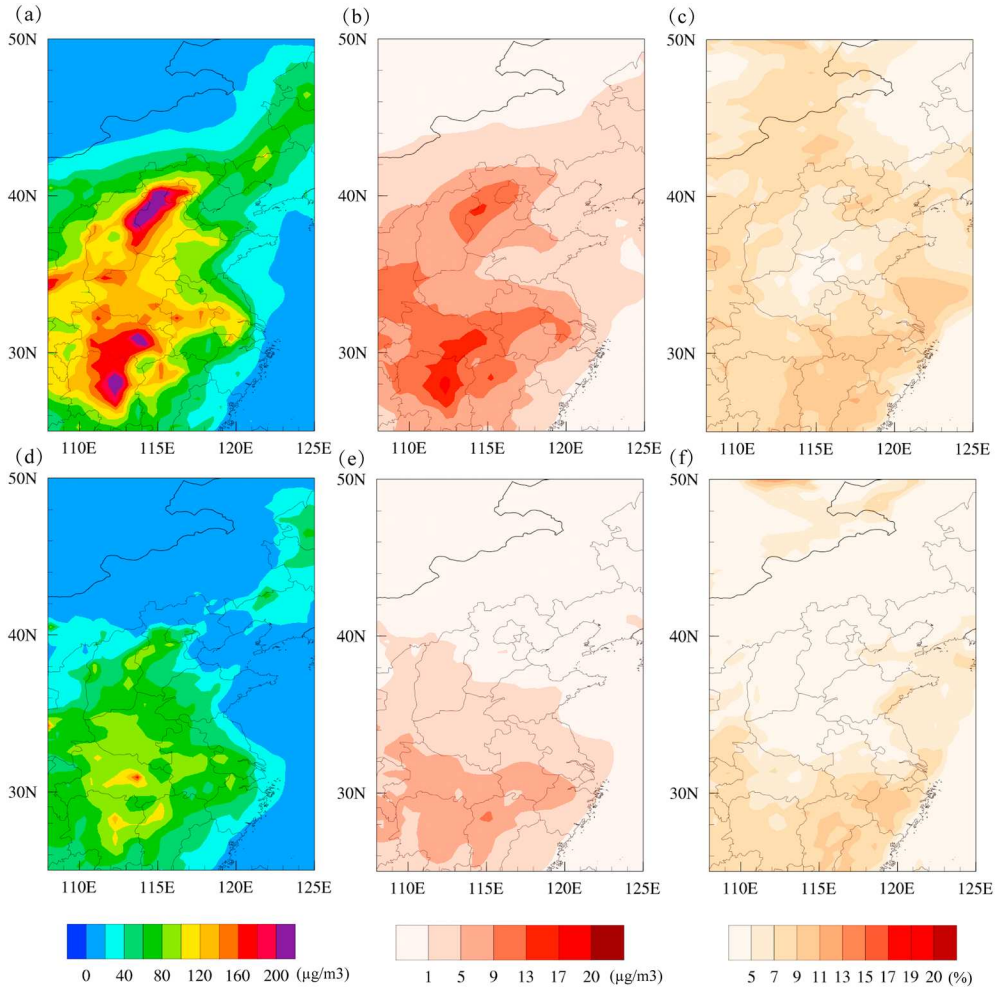


**Figure 12.** Same as Figure 11 but for particulate matter $PM_{2.5}$.

those reported as 189.6, 84, and 5.3% for $NO_3^-$, $NH_4^+$, and $SO_4^{2-}$, respectively. The total response of $PM_{2.5}$ to the $NH_3$ changes (Figure 12) is in the range of 25 to 55% (5–11% per 20% $NH_3$ increase) over the NCP. The average concentrations of inorganic aerosols and $PM_{2.5}$ in different scenario simulations under polluted and clean conditions in Beijing are listed in Table 1. Large differences between CTL and IncNH3 in the polluted case are found in Beijing. The relative changes for $NH_4^+$, $SO_4^{2-}$, $NO_3^-$, and $PM_{2.5}$ are in the range of the regional values, 13%, 4%, 23%, and 8%, respectively. It implies that $NH_3$ is one of the key factors that influence the $PM_{2.5}$ formation under current NCP conditions during heavy haze periods. In clean cases, however, all inorganic aerosols are insensitive to changes in $NH_3$ emission, with the relative variation

**Table 1**
*Averaged Concentrations of $PM_{2.5}$ ($\mu g/m^3$) in Different Scenario Simulation Under Polluted and Clean Conditions at the Site of IAP Tower*

| Species | CTL in polluted case | IncNH$_3$ in polluted case | % | CTL in clean case | IncNH$_3$ in clean case | % |
|---|---|---|---|---|---|---|
| $NH_4^+$ | 19.58 | 22.20 | 13 | 2.69 | 2.88 | 7 |
| $SO_4^{2-}$ | 27.54 | 28.61 | 4 | 2.63 | 2.66 | 1 |
| $NO_3^-$ | 32.42 | 40.00 | 23 | 5.86 | 6.48 | 11 |
| $PM_{2.5}$ | 172.89 | 186.78 | 8 | 42.54 | 44.87 | 5 |

Abbreviation: IAP. Institute of Atmospheric Physics.

lower than 5%. Fu et al. (2017) also indicated that it is more effective for PM reduction to control $NH_3$ emission under high level of $SO_2$ and $NO_x$ emissions conditions.

## 4. Summary

This paper presents measurement results of hourly atmospheric $NH_3$, $H^+$, AWC, $PM_{2.5}$, and inorganic aerosol components (sulfate, nitrate, and ammonium) of $PM_{2.5}$ during the winter APHH campaign in Beijing. The highest concentration of hourly $PM_{2.5}$ reached 633 $\mu g/m^3$ during the campaign. The variations of all the species are self-consistent and reasonable expressed.

In order to better understand the effects of the $NH_3$ to air pollution in Beijing, the whole period of the campaign was separated into polluted and nonpolluted episodes according to the concentrations of $PM_{2.5}$. Compared with the nonpolluted episodes, the polluted periods are characterized as having more acidic particles, low excess $NH_x$, and higher AWC. The results clearly indicated more $NH_3$ entering into the particle $NH_4^+$ under the large amount of AWC and hence causing the high concentration of $PM_{2.5}$ during the winter haze pollution.

The leading factor for the haze pollution over the NCP is investigated using ISORROPIA II thermodynamic model as well as the theoretically calculation of the pathway for $NO_x$ to $NO_3^-$. Excess $NH_x$ is found to increase the formation of $NH_4NO_3$ especially during the nighttime reactions, which triggers the decrease of aerosol DRH down to less than 50%, causes the formation of AWC even under RH conditions lower than 50% and preconditions the aerosol particles for rapid heterogeneous reactions. Once the aerosol particles become wet, a further increase of RH enlarges the positive feedback "AWC-heterogeneous reactions," which ultimately leads to the formation of severe haze. Although our finding has been obtained by analyzing measurements from a site in Beijing, it may also be applicable to other regions with similar emissions and meteorological conditions.

Finally, sensitively simulations were performed using the 3-D numerical model NAQPMS and carefully validated using observation data. Our NAQPMS model simulations show that inorganic aerosols enhancements are more sensitive to $NH_3$ increase in polluted conditions than in nonpolluted periods. Therefore, $NH_3$ is one of the key factors that influence SIAs formation in the NCP during heavy haze periods.

**Acknowledgments**
This study was financially supported by the National Natural Science Foundation of China (grants 41877313, 41571130024, 91744206 and 41575123) and Basic Research Fund of CAMS (2016Z001). The data used in this paper are available in https://www.pangaea.de/.

## References

Athanasopoulou, E., Tombrou, M., Pandis, S. N., & Russell, A. G. (2008). The role of sea-salt emissions and heterogeneous chemistry in the air quality of polluted coastal areas. *Atmospheric Chemistry and Physics*, *8*(19), 5755–5769. https://doi.org/10.5194/acp-8-5755-2008

Bian, Y. X., Zhao, C. S., Ma, N., Chen, J., & Xu, W. Y. (2014). A study of aerosol liquid water content based on hygroscopicity measurements at high relative humidity in the North China Plain. *Atmospheric Chemistry and Physics*, *14*(12), 6417–6426. https://doi.org/10.5194/acp-14-6417-2014

Bin Babar, Z., Park, J. H., & Lim, H. J. (2017). Influence of $NH_3$ on secondary organic aerosols from the ozonolysis and photooxidation of alpha-pinene in a flow reactor. *Atmospheric Environment*, *164*, 71–84. https://doi.org/10.1016/j.atmosenv.2017.05.034

Bougiatioti, A., Nikolaou, P., Stavroulas, I., Kouvarakis, G., Weber, R., Nenes, A., et al. (2016). Particle water and pH in the eastern Mediterranean: source variability and implications for nutrient availability. *Atmospheric Chemistry and Physics*, *16*(7), 4579–4591. https://doi.org/10.5194/acp-16-4579-2016

Byun, D. W., & Dennis, R. (1995). Design artifacts in Eulerian air-quality models—Evaluation of the effects of layer thickness and vertical profile correction on surface ozone concentrations. *Atmospheric Environment*, *29*(1), 105–126. https://doi.org/10.1016/1352-2310(94)00225-A

Cao, J. J., Zhang, T., Chow, J. C., Watson, J. G., Wu, F., & Li, H. (2009). Characterization of atmospheric ammonia over Xi'an, China. *Aerosol and Air Quality Research*, *9*(2), 277–289. https://doi.org/10.4209/aaqr.2008.10.0043

Cheng, Y. F., Zheng, G., Wei, C., Mu, Q., Zheng, B., Wang, Z., et al. (2016). Reactive nitrogen chemistry in aerosol water as a source of sulfate during haze events in China. *Science Advances*, *2*, e1601530. https://doi.org/10.1126/sciadv.1601530

Duan, F. K., He, K. B., Ma, Y. L., Ihozaki, T., Kawasaki, H., Arakawa, R., et al. (2016). High molecular weight organic compounds (HMWOCs) in severe winter haze: Direct observation and insights on the formation mechanism. *Environmental Pollution*, *218*, 289–296. https://doi.org/10.1016/j.envpol.2016.07.004

Fountoukis, C., & Nenes, A. (2007). ISORROPIA II: A computationally efficient thermodynamic equilibrium model for $K^+$-$Ca^{2+}$-$Mg^{2+}$-Nh(4)(+)-$Na^+$-$SO_4^{2-}$-$NO_3^-$-$Cl^-$-H2O aerosols. *Atmospheric Chemistry and Physics*, *7*(17), 4639–4659. https://doi.org/10.5194/acp-7-4639-2007

Fu, X., Wang, S. X., Xing, J., Zhang, X. Y., Wang, T., & Hao, J. M. (2017). Increasing ammonia concentrations reduce the effectiveness of particle pollution control achieved via $SO_2$ and $NO_X$ emissions reduction in East China. *Environmental Science & Technology Letters*, *4*(6), 221–227. https://doi.org/10.1021/acs.estlett.7b00143

Gao, M., Carmichael, G. R., Saide, P. E., Lu, Z. F., Yu, M., Streets, D. G., & Wang, Z. F. (2016). Response of winter fine particulate matter concentrations to emission and meteorology changes in North China. *Atmospheric Chemistry and Physics*, *16*(18), 11,837–11,851. https://doi.org/10.5194/acp-16-11837-2016

Ge, B., Wang, Z., Lin, W., Xu, X., Li, J., Ji, D., & Ma, Z. (2018). Air pollution over the North China Plain and its implication of regional transport: A new sight from the observed evidences. *Environmental Pollution*, *234*(Supplement C), 29–38. https://doi.org/10.1016/j.envpol.2017.10.084

Ge, B. Z., Sun, Y. L., Liu, Y., Dong, H. B., Ji, D. S., Jiang, Q., et al. (2013). Nitrogen dioxide measurement by cavity attenuated phase shift spectroscopy (CAPS) and implications in ozone production efficiency and nitrate formation in Beijing, China. *Journal of Geophysical Research: Atmospheres*, *118*, 9499–9509. https://doi.org/10.1002/jgrd.50757

Ge, B. Z., Wang, Z. F., Xu, X. B., Wu, J. B., Yu, X. L., & Li, J. (2014). Wet deposition of acidifying substances in different regions of China and the rest of East Asia: Modeling with updated NAQPMS. *Environmental Pollution*, *187*, 10–21. https://doi.org/10.1016/j.envpol.2013.12.014

Ge, B. Z., Xu, X. B., Lin, W. L., Li, J., & Wang, Z. F. (2012). Impact of the regional transport of urban Beijing pollutants on downwind areas in summer: ozone production efficiency analysis. *Tellus B*, *64*(1). https://doi.org/10.3402/tellusb.v64i0.17348

Guenther, A., Karl, T., Harley, P., Wiedinmyer, C., Palmer, P. I., & Geron, C. (2006). Estimates of global terrestrial isoprene emissions using MEGAN (Model of Emissions of Gases and Aerosols from Nature). *Atmospheric Chemistry and Physics*, *6*(11), 3181–3210. https://doi.org/10.5194/acp-6-3181-2006

Guo, H., Xu, L., Bougiatioti, A., Cerully, K. M., Capps, S. L., Hite, J. R. Jr., et al. (2015). Fine-particle water and pH in the southeastern United States. *Atmospheric Chemistry and Physics*, *15*(9), 5211–5228. https://doi.org/10.5194/acp-15-5211-2015

Guo, H. Y., Liu, J. M., Froyd, K. D., Roberts, J. M., Veres, P. R., Hayes, P. L., et al. (2017). Fine particle pH and gas-particle phase partitioning of inorganic species in Pasadena, California, during the 2010 CalNex campaign. *Atmospheric Chemistry and Physics*, *17*(9), 5703–5719. https://doi.org/10.5194/acp-17-5703-2017

Hao, J. Q., Ge, B. Z., Wang, Z. F., Zhang, X. Z., Tang, L. L., & Xu, D. H. (2017). Observational study of air pollution complex in Nanjing in June 2014 (In Chinese with English abstract). *Environmental Sciences*, *9*, 3585–3593.

Hauglustaine, D. A., Brasseur, G. P., Walters, S., Rasch, P. J., Muller, J. F., Emmons, L. K., & Carroll, C. A. (1998). MOZART, a global chemical transport model for ozone and related chemical tracers 2. Model results and evaluation. *Journal of Geophysical Research-Atmospheres*, *103*(D21), 28,291–28,335. https://doi.org/10.1029/98JD02398

He, K., Zhao, Q., Ma, Y., Duan, F., Yang, F., Shi, Z., & Chen, G. (2012). Spatial and seasonal variability of PM2.5 acidity at two Chinese megacities: insights into the formation of secondary inorganic aerosols. *Atmospheric Chemistry and Physics*, *12*(3), 1377–1395. https://doi.org/10.5194/acp-12-1377-2012

He, P., Alexander, B., Geng, L., Chi, X., Fan, S., Zhan, H., et al. (2018). Isotopic constraints on heterogeneous sulfate production in Beijing haze. *Atmospheric Chemistry and Physics*, *18*(8), 5515–5528. https://doi.org/10.5194/acp-18-5515-2018

Hernandez, D. L., Vallano, D. M., Zavaleta, E. S., Tzankova, Z., Pasari, J. R., Weiss, S., et al. (2016). Nitrogen Pollution is Linked to US Listed Species Declines. *Bioscience*, *66*(3), 213–222. https://doi.org/10.1093/biosci/biw003

Hu, G. Y., Zhang, Y. M., Sun, J. Y., Zhang, L. M., Shen, X. J., Lin, W. L., & Yang, Y. (2014). Variability, formation and acidity of water-soluble ions in PM2.5 in Beijing based on the semi-continuous observations. *Atmospheric Research*, *145*, 1–11.

Huo, Q., Cai, X. H., Kang, L., Zhang, H. S., Song, Y., & Zhu, T. (2015). Estimating ammonia emissions from a winter wheat cropland in North China Plain with field experiments and inverse dispersion modeling. *Atmospheric Environment*, *104*, 1–10. https://doi.org/10.1016/j.atmosenv.2015.01.003

King, D. W., & Kester, D. R. (1989). Determination of seawater Ph from 1.5 to 8.5 using colorimetric indicators. *Marine Chemistry*, *26*(1), 5–20. https://doi.org/10.1016/0304-4203(89)90061-3

Lachatre, M., Fortems-Cheiney, A., Foret, G., Siour, G., Dufour, G., Clarisse, L., et al. (2019). The unintended consequence of $SO_2$ and $NO_2$ regulations over China: increase of ammonia levels and impact on $PM_{2.5}$ concentrations. *Atmospheric Chemistry and Physics*, *19*(10), 6701–6716. https://doi.org/10.5194/acp-19-6701-2019

Li, J., Wang, Z., Zhuang, G., Luo, G., Sun, Y., & Wang, Q. (2012). Mixing of Asian mineral dust with anthropogenic pollutants over East Asia: A model case study of a super-duststorm in March 2010. *Atmospheric Chemistry and Physics*, *12*(16), 7591–7607. https://doi.org/10.5194/acp-12-7591-2012

Li, M., Zhang, Q., Kurokawa, J. I., Woo, J. H., He, K., Lu, Z., et al. (2017). MIX: A mosaic Asian anthropogenic emission inventory under the international collaboration framework of the MICS-Asia and HTAP. *Atmospheric Chemistry and Physics*, *17*(2), 935–963. https://doi.org/10.5194/acp-17-935-2017

Lin, W., Xu, X., Ge, B., & Zhang, X. (2009). Characteristics of gaseous pollutants at Gucheng, a rural site southwest of Beijing. *Journal of Geophysical Research*, *114*, D00G14. https://doi.org/10.1029/2008JD010339

Lin, W., Xu, X., Zhang, X., & Tang, J. (2008). Contributions of pollutants from north china plain to surface ozone at the shangdianzi GAW station. *Atmospheric Chemistry and Physics*, *8*(19), 5889–5898. https://doi.org/10.5194/acp-8-5889-2008

Liu, M., Huang, X., Song, Y., Xu, T., Wang, S., Wu, Z., et al. (2018). Rapid $SO_2$ emission reductions significantly increase tropospheric ammonia concentrations over the North China Plain. *Atmospheric Chemistry and Physics*, *18*(24), 17,933–17,943. https://doi.org/10.5194/acp-18-17933-2018

Liu, M. X., Song, Y., Zhou, T., Xu, Z. Y., Yan, C. Q., Zheng, M., et al. (2017). Fine particle pH during severe haze episodes in northern China. *Geophysical Research Letters*, *44*, 5213–5221. https://doi.org/10.1002/2017GL073210

Liu, X. J., Zhang, Y., Han, W., Tang, A., Shen, J., Cui, Z., et al. (2013). Enhanced nitrogen deposition over China. *Nature*, *494*(7438), 459–462. https://doi.org/10.1038/nature11917

Malaguti, A., Mircea, M., La Torretta, T. M. G., Telloli, C., Petralia, E., Stracquadanio, M., & Berico, M. (2015). Comparison of online and offline methods for measuring fine secondary inorganic ions and carbonaceous aerosols in the Central Mediterranean Area. *Aerosol and Air Quality Research*, *15*(7), 2641–2653. https://doi.org/10.4209/aaqr.2015.04.0240

Meng, Z. Y., Lin, W. L., Jiang, X. M., Yan, P., Wang, Y., Zhang, Y. M., et al. (2011). Characteristics of atmospheric ammonia over Beijing, China. *Atmospheric Chemistry and Physics*, *11*(12), 6139–6151. https://doi.org/10.5194/acp-11-6139-2011

Meng, Z. Y., Xu, X. B., Wang, T., Zhang, X. Y., Yu, X. L., Wang, S. F., et al. (2010). Ambient sulfur dioxide, nitrogen dioxide, and ammonia at ten background and rural sites in China during 2007-2008. *Atmospheric Environment*, *44*(21-22), 2625–2631. https://doi.org/10.1016/j.atmosenv.2010.04.008

Meng, Z. Y., Xu, X., Lin, W., Ge, B., Xie, Y., Song, B., et al. (2018). Role of ambient ammonia in particulate ammonium formation at a rural site in the North China Plain. *Atmospheric Chemistry and Physics*, *18*(1), 167–184. https://doi.org/10.5194/acp-18-167-2018

Na, K., Song, C., Switzer, C., & Cocker, D. R. (2007). Effect of ammonia on secondary organic aerosol formation from alpha-Pinene ozonolysis in dry and humid conditions. *Environmental Science & Technology*, *41*(17), 6096–6102. https://doi.org/10.1021/es061956y

Nenes, A., Pandis, S. N., & Pilinis, C. (1998). ISORROPIA: A new thermodynamic equilibrium model for multiphase multicomponent inorganic aerosols. *Aquatic Geochemistry*, *4*(1), 123–152. https://doi.org/10.1023/A:1009604003981

Odum, J. R., Jungkamp, T. P. W., Griffin, R. J., Forstner, H. J. L., Flagan, R. C., & Seinfeld, J. H. (1997). Aromatics, reformulated gasoline, and atmospheric organic aerosol formation. *Environmental Science & Technology*, *31*(7), 1890–1897. https://doi.org/10.1021/es960535l

Pan, Y., Tian, S., Zhao, Y., Zhang, L., Zhu, X., Gao, J., et al. (2018). Identifying ammonia hotspots in China using a national observation network. *Environmental Science & Technology*, *52*(7), 3926–3934. https://doi.org/10.1021/acs.est.7b05235

Pan, Y. P., Wang, Y. S., Tang, G. Q., & Wu, D. (2012). Wet and dry deposition of atmospheric nitrogen at ten sites in Northern China. *Atmospheric Chemistry and Physics*, *12*(14), 6515–6535. https://doi.org/10.5194/acp-12-6515-2012

Pathak, R. K., Wu, W. S., & Wang, T. (2009). Summertime PM2.5 ionic species in four major cities of China: nitrate formation in an ammonia-deficient atmosphere. *Atmospheric Chemistry and Physics*, *9*(5), 1711–1722. https://doi.org/10.5194/acp-9-1711-2009

Pathak, R. K., Yao, X. H., & Chan, C. K. (2004). Sampling artifacts of acidity and ionic species in PM2.5. *Environmental Science & Technology*, *38*(1), 254–259. https://doi.org/10.1021/es0342244

Ryerson, T. B., Andrews, A. E., Angevine, W. M., Bates, T. S., Brock, C. A., Cairns, B., et al. (2013). The 2010 California Research at the Nexus of Air Quality and Climate Change (CalNex) field study. *Journal of Geophysical Research: Atmospheres*, *118*, 5830–5866. https://doi.org/10.1002/jgrd.50331

Seinfeld, J. H., & Pandis, S. N. (2006). *Atmospheric chemistry and physics: From air pollution to climate change*. New York: Wiley.

Sheppard, L. J., Leith, I. D., Mizunuma, T., Cape, J. N., Crossley, A., Leeson, S., et al. (2011). Dry deposition of ammonia gas drives species change faster than wet deposition of ammonium ions: Evidence from a long-term field manipulation. *Global Change Biology*, *17*(12), 3589–3607. https://doi.org/10.1111/j.1365-2486.2011.02478.x

Song, S., Gao, M., Xu, W., Shao, J., Shi, G., Wang, S., et al. (2018). Fine-particle pH for Beijing winter haze as inferred from different thermodynamic equilibrium models. *Atmospheric Chemistry and Physics*, *18*(10), 7423–7438. https://doi.org/10.5194/acp-18-7423-2018

Stockwell, W. R., Middleton, P., Chang, J. S., & Tang, X. Y. (1990). The 2nd generation regional acid deposition model chemical mechanism for regional air-quality modeling. *Journal of Geophysical Research-Atmospheres*, *95*(D10), 16,343–16,367. https://doi.org/10.1029/JD095iD10p16343

Sun, Y. L., Wang, Z. F., Dong, H. B., Yang, T., Li, J., Pan, X. L., et al. (2012). Characterization of summer organic and inorganic aerosols in Beijing, China with an Aerosol Chemical Speciation Monitor. *Atmospheric Environment*, *51*, 250–259. https://doi.org/10.1016/j.atmosenv.2012.01.013

Sun, Y. L., Wang, Z. F., Du, W., Zhang, Q., Wang, Q. Q., Fu, P. Q., et al. (2015). Long-term real-time measurements of aerosol particle composition in Beijing, China: seasonal variations, meteorological effects, and source analysis. *Atmospheric Chemistry and Physics*, *15*(17), 10,149–10,165. https://doi.org/10.5194/acp-15-10149-2015

Sun, Y. L., Zhang, Q., Schwab, J. J., Chen, W. N., Bae, M. S., Lin, Y. C., et al. (2011). A case study of aerosol processing and evolution in summer in New York City. *Atmospheric Chemistry and Physics*, *11*(24), 12,737–12,750. https://doi.org/10.5194/acp-11-12737-2011

Tang, G., Zhang, J., Zhu, X., Song, T., Münkel, C., Hu, B., et al. (2016). Mixing layer height and its implications for air pollution over Beijing, China. *Atmospheric Chemistry and Physics*, *16*(4), 2459–2475. https://doi.org/10.5194/acp-16-2459-2016

Uno, I., Yumimoto, K., Osada, K., Wang, Z., Pan, X. L., Itahashi, S., & Yamamoto, S. (2017). Dust acid uptake analysis during long-lasting dust and pollution episodes over East Asia based on synergetic observation and chemical transport model. *Solaiat*, *13*(0), 109–113. https://doi.org/10.2151/sola.2017-020

van der Werf, G. R., Randerson, J. T., Giglio, L., Collatz, G. J., Kasibhatla, P. S., & Arellano, A. F. (2006). Interannual variability in global biomass burning emissions from 1997 to 2004. *Atmospheric Chemistry and Physics*, *6*(11), 3423–3441. https://doi.org/10.5194/acp-6-3423-2006

Walcek, C. J., & Aleksic, N. M. (1998). A simple but accurate mass conservative, peak-preserving, mixing ratio bounded advection algorithm with Fortran code. *Atmospheric Environment*, *32*(22), 3863–3880. https://doi.org/10.1016/S1352-2310(98)00099-5

Walker, J. T., Whitall, D. R., Robarge, W., & Paerl, H. W. (2004). Ambient ammonia and ammonium aerosol across a region of variable ammonia emission density. *Atmospheric Environment*, *38*(9), 1235–1246. https://doi.org/10.1016/j.atmosenv.2003.11.027

Wang, G. H., Zhang, R., Gomez, M. E., Yang, L., Zamora, M. L., Hu, M., et al. (2016). Persistent sulfate formation from London Fog to Chinese haze. *Proceedings of the National Academy of Sciences of the United States of America*, *113*(48), 13,630–13,635. https://doi.org/10.1073/pnas.1616540113

Wang, S. X., & Hao, J. M. (2012). Air quality management in China: Issues, challenges, and options. *Journal of Environmental Sciences*, *24*(1), 2–13. https://doi.org/10.1016/S1001-0742(11)60724-9

Wang, Z., Itahashi, S., Uno, I., Pan, X. L., Osada, K., Yamamoto, S., et al. (2017). Modeling the long-range transport of particulate matters for January in East Asia using NAQPMS and CMAQ. *Aerosol and Air Quality Research*, *17*(12), 3064–3078. https://doi.org/10.4209/aaqr.2016.12.0534

Wang, Z., Maeda, T., Hayashi, M., Hsiao, L. F., & Liu, K. Y. (2001). A nested air quality prediction modeling system for urban and regional scales: Application for high-ozone episode in Taiwan. *Water, Air, and Soil Pollution*, *130*(1/4), 391–396. https://doi.org/10.1023/A:1013833217916

Wang, Z., Pan, X., Uno, I., Li, J., Wang, Z., Chen, X., et al. (2017). Significant impacts of heterogeneous reactions on the chemical composition and mixing state of dust particles: A case study during dust events over northern China. *Atmospheric Environment*, *159*, 83–91. https://doi.org/10.1016/j.atmosenv.2017.03.044

Wang, Z., Pan, X. L., Uno, I., Chen, X. S., Yamamoto, S., Zheng, H. T., et al. (2018). Importance of mineral dust and anthropogenic pollutants mixing during a long-lasting high PM event over East Asia. *Environmental Pollution*, *234*, 368–378. https://doi.org/10.1016/j.envpol.2017.11.068

Warner, J. X., Dickerson, R. R., Wei, Z., Strow, L. L., Wang, Y., & Liang, Q. (2017). Increased atmospheric ammonia over the world's major agricultural areas detected from space. *Geophysical Research Letters*, *44*, 2875–2884. https://doi.org/10.1002/2016GL072305

Weber, R. J., Guo, H. Y., Russell, A. G., & Nenes, A. (2016). High aerosol acidity despite declining atmospheric sulfate concentrations over the past 15 years. *Nature Geoscience*, *9*(4), 282–285. https://doi.org/10.1038/ngeo2665

Wesely, M. L. (1989). Parameterization of Surface Resistances to Gaseous Dry Deposition in Regional-Scale Numerical-Models. *Atmospheric Environment*, *23*(6), 1293–1304. https://doi.org/10.1016/0004-6981(89)90153-4

Wu, Z. J., Wang, Y., Tan, T., Zhu, Y., Li, M., Shang, D., et al. (2018). Aerosol liquid water driven by anthropogenic inorganic salts: Implying its key role in haze formation over the North China Plain. *Environmental Science & Technology Letters*, *5*(3), 160–166. https://doi.org/10.1021/acs.estlett.8b00021

Xia, Y. M., Zhao, Y., & Nielsen, C. P. (2016). Benefits of of China's efforts in gaseous pollutant control indicated by the bottom-up emissions and satellite observations 2000-2014. *Atmospheric Environment*, *136*, 43–53. https://doi.org/10.1016/j.atmosenv.2016.04.013

Xiang, Y., Zhang, T., Liu, J., Lv, L., Dong, Y., & Chen, Z. (2019). Atmosphere boundary layer height and its effect on air pollutants in Beijing during winter heavy pollution. *Atmospheric Research*, *215*, 305–316. https://doi.org/10.1016/j.atmosres.2018.09.014

Xu, D., Ge, B., Wang, Z., Sun, Y., Chen, Y., Ji, D., et al. (2017). Below-cloud wet scavenging of soluble inorganic ions by rain in Beijing during the summer of 2014. *Environmental Pollution*, *230*(Supplement C), 963–973. https://doi.org/10.1016/j.envpol.2017.07.033

Yue, D., Hu, M., & Wu, Z. (2013). Variation and interaction of major azotic inorganic compounds in the summer in beijing (in Chinese). *Environmental Monitoring in China*, *29*, 9–14.

Zaveri, R. A., & Peters, L. K. (1999). A new lumped structure photochemical mechanism for large-scale applications. *Journal of Geophysical Research-Atmospheres*, *104*(D23), 30,387–30,415. https://doi.org/10.1029/1999JD900876

Zhang, L. M., Gong, S. L., Padro, J., & Barrie, L. (2001). A size-segregated particle dry deposition scheme for an atmospheric aerosol module. *Atmospheric Environment*, *35*(3), 549–560. https://doi.org/10.1016/S1352-2310(00)00326-5

Zhang, Q., Jimenez, J. L., Worsnop, D. R., & Canagaratna, M. (2007). A case study of urban particle acidity and its influence on secondary organic aerosol. *Environmental Science & Technology*, *41*(9), 3213–3219. https://doi.org/10.1021/es061812j

Zheng, B., Tong, D., Li, M., Liu, F., Hong, C., Geng, G., et al. (2018). Trends in China's anthropogenic emissions since 2010 as the consequence of clean air actions. *Atmospheric Chemistry and Physics Discussions*, *2018*, 1–27. https://doi.org/10.5194/acp-2018-374